Biogeosciences, 12, 1–14, 2015
www.biogeosciences.net/12/1/2015/
doi:10.5194/bg-12-1-2015

Biogeosciences
Open Access

Spatiotemporal variations of nitrogen isotopic records in the Arabian Sea

S.-J. Kao[1], B.-Y. Wang[1], L.-W. Zheng[1], K. Selvaraj[1], S.-C. Hsu[2], X. H. Sean Wan[1], M. Xu[1], and C.-T. Arthur Chen[3]

[1]State Key Laboratory of Marine Environmental Science, Xiamen University, Xiamen, China
[2]Research Center for Environmental Changes, Academia Sinica, Taipei, Taiwan
[3]Department of Oceanography, National Sun Yat-sen University, Kaohsiung, Taiwan

Correspondence to: S.-J. Kao (sjkao@xmu.edu.cn)

Received: 3 May 2014 – Published in Biogeosciences Discuss.: 11 June 2014
Revised: 22 October 2014 – Accepted: 10 November 2014 – Published: 5 January 2015

Abstract. Available reports of dissolved oxygen, δ^{15}N of nitrate ($\delta^{15}N_{NO_3}$) and δ^{15}N of total nitrogen ($\delta^{15}N_{bulk}$) for trap material and surface/downcore sediments from the Arabian Sea (AS) were synthesized to explore the AS' past nitrogen dynamics. Based on 25 µmol kg^{-1} dissolved oxygen isopleth at a depth of 150 m, we classified all reported data into northern and southern groups. By using $\delta^{15}N_{bulk}$ of the sediments, we obtained geographically distinctive bottom-depth effects for the northern and southern AS at different climate stages. After eliminating the bias caused by bottom depth, the modern-day sedimentary $\delta^{15}N_{bulk}$ values largely reflect the $\delta^{15}N_{NO_3}$ supply from the bottom of the euphotic zone. Additionally to the data set, nitrogen and carbon contents vs. their isotopic compositions of a sediment core (SK177/11) collected from the most southeastern part of the AS were measured for comparison. We found a one-step increase in $\delta^{15}N_{bulk}$ starting at the deglaciation with a corresponding decrease in $\delta^{13}C_{TOC}$ similar to reports elsewhere revealing a global coherence. By synthesizing and reanalyzing all reported down core $\delta^{15}N_{bulk}$, we derived bottom-depth correction factors at different climate stages, respectively, for the northern and southern AS. The diffusive sedimentary $\delta^{15}N_{bulk}$ values in compiled cores became confined after bias correction revealing a more consistent pattern except recent 6 ka. Such high similarity to the global temporal pattern indicates that the nitrogen cycle in the entire AS had responded to open-ocean changes until 6 ka BP. Since 6 ka BP, further enhanced denitrification (i.e., increase in $\delta^{15}N_{bulk}$) in the northern AS had occurred and was likely driven by monsoon, while, in the southern AS, we observed a synchronous reduction in $\delta^{15}N_{bulk}$, implying that nitrogen fixation was promoted correspondingly as the intensification of local denitrification at the northern AS basin.

1 Introduction

Biogeochemical processes of nitrogen in the ocean are intimately related to various elemental cycles (synergistically modulate atmospheric CO_2 and N_2O concentrations), hence the feedback on the climate being on a millennial time scale (Gruber, 2004; Falkowski and Godfrey, 2008; Altabet et al., 2002). Though oxygen deficient zones (ODZs) occupy only ∼ 4 % of ocean volume, the denitrification process therein contributes remarkably to the losses of nitrate, leaving excess P in the remaining water mass to stimulate N_2 fixation while entering the euphotic zone (Morrison et al., 1998; Deutsch et al., 2007) and thus controlling the budget of bioavailable nitrogen in ocean. Denitrification leaves $^{15}NO_3^-$ in residual nitrate (Sigman et al., 2001), whereas N_2 fixation introduces new bioavailable nitrogen with low δ^{15}N values (Capone et al., 1997) into ocean for compensation. The Arabian Sea (AS) – one of the three largest ODZs in the world ocean with distinctive monsoon driven upwelling – accounts for at least one-third of the loss of marine fixed nitrogen (Codispoti and Christensen, 1985) playing an important role in the past climate via regulating atmospheric N_2O concentration (Agnihotri et al., 2006) or nitrogen inventory to modulate CO_2 sequestration through a biological pump (Altabet, 2006).

Sedimentary nitrogen isotope, measured as standard δ notation, with respect to standards of atmospheric nitrogen, is an important tool to study the past marine nitrogen cycle.

Nitrogen isotope compositions of sedimentary organic matter potentially reflect biological processes in water columns, such as denitrification (Altabet et al., 1995; Ganeshram et al., 1995, 2000), nitrogen fixation (Haug et al., 1998), and the degree of nitrate utilization by algae (Altabet and Francois, 1994; Holmes et al., 1996; Robinson et al., 2004). However, alteration may occur (through various ways or processes; e.g., diagenesis) before the signal of δ^{15}N of exported production is buried.

Previous measurements of $\delta^{15}N_{bulk}$ in various cores and surface sediments in the AS showed the following points: (1) near-surface NO_3^- in the AS is completely utilized in an annual cycle, resulting in small isotopic fractionation between δ^{15}N of exported sinking particles and δ^{15}N of NO_3^- supplied to the euphotic zone (Altabet, 1988; Thunell et al., 2004); (2) monsoon-driven surface productivity and associated oxidant demand were regarded as the main control on water column denitrification in the past (Ganeshram et al., 2000; Ivanochko et al., 2005); (3) sedimentary $\delta^{15}N_{bulk}$ primarily reflects the relative intensity of water column denitrification in this area (Altabet et al., 1995, 1999); (4) oxygen supply at intermediate depth by the Antarctic intermediate waters (AAIWs) can modulate the denitrification intensity in the northern AS (Schulte et al., 1999; Schmittner et al., 2007; Pichevin et al., 2007). Among previous research, the geographical features in sedimentary $\delta^{15}N_{bulk}$ between the north and south basins of the AS have not been discussed, particularly on the basis of bottom-depth effect, which might be different during glacial and interglacial periods.

In this study, a sediment core (SK177/11) collected from the slope of the southeastern AS was measured for organic C and N contents and their stable isotopes. We synthesized previous hydrographical and isotopic data, such as dissolved oxygen (DO), N^* ($N^* = NO_3^- 16 \times PO_4^{3-} + 2.9$; Gruber and Sarmiento, 2002), and δ^{15}N of nitrate, as well as trapped material and surface/downcore sediments, among which surface and downcore sediments may have experienced more intensified diagenetic alteration. Based on the subsurface of a DO concentration of 25 µmol kg^{-1} isopleth at 150 m, the data sets in the AS were separated into north and south basins by time span (glacial, Holocene and modern) for comparison. We aim to (1) investigate the geographic and glacial–interglacial differences in bottom-depth effect and to (2) retrieve extra information from sedimentary $\delta^{15}N_{bulk}$ by removing basin/climate stage specific bottom-depth effects, thus better deciphering the environmental history of the Arabian Sea.

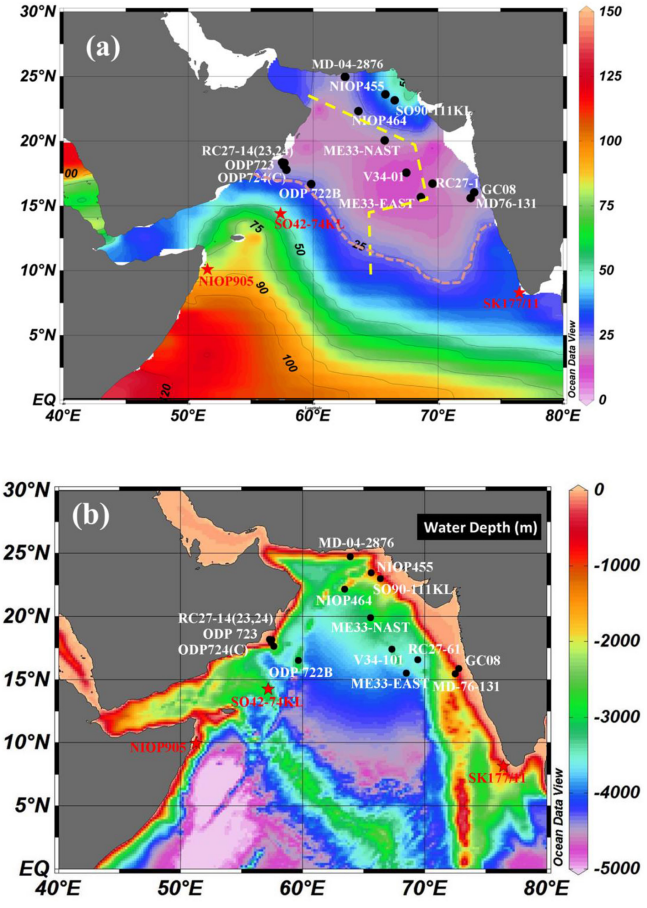

Figure 1. (a) Map of the Arabian Sea. Dissolved oxygen (DO) concentration at 150 m (World Ocean Atlas 09) was shown in color contour. Southern (⋆) and northern (•) categories of available cores and SK177/11, in this study, were defined by DO of 25 µmol kg^{-1} (see text; purple dash curve). **(b)** Bathymetric map superimposed by core locations; **(c)**, **(d)** and **(e)** are DO, nitrate and N^* transects (yellow dashed line in **(a)**, online data originated from cruises of JGOFS in 1995), respectively, for upper 2000 m. **(f)** N^* transect for the upper 300 m with arrows revealing the flow direction. In **(a)**, the northern cores include core MD-04-2876 (828 m; Pichevin et al., 2007), core NIOP455 vs. NIOP464 (1002 m vs. 1470 m; Reichart et al., 1998), SO90-111KL vs. ME33-NAST(775 m vs. 3170 m; Suthhof et al., 2001), ODP724C vs. ME33-EAST (603 m vs. 3820 m; Möbius et al., 2011), RC27-24 vs. RC27-61 (1416 m vs. 1893 m; Altabet et al., 1995), ODP723, ODP722(B) vs. V34-101 (808 m, 2028 m vs. 3038 m; Altabet et al., 1999), RC27-14 vs. RC27-23 (596 m vs. 820 m; Altabet et al., 2002), GC08 (2500 m; Banakar et al., 2005), MD-76-131 (1230 m; Ganeshram et al., 2000); the southern cores include core SO42-74KL (3212 m; Suthhof et al., 2001), NIOP905 (1586 m; Ivanochko et al., 2005) and SK177/11 (776 m; this study).

2 Study area

The Arabian Sea is characterized by seasonal reversal of monsoon winds, resulting in large seasonal physical/hydrographic/biological/chemical variations in water columns (Nair et al., 1989). Cold and dry northeasterly winds blow during winter from a high-pressure cell of the Tibetan Plateau, whereas heating of the Tibetan Plateau in summer (June to September) reverses the pressure gradient leading to warm and moist southwesterly winds and

Table 1. Accelerator mass spectrometry (AMS) ^{14}C dates of sediment core SK177/11. Radiocarbon ages were calibrated using the CALIB 6.0 program (http://calib.qub.ac.uk/calib/calib.html, Reimer et al., 2009).

Lab code	Depth cm	Dating materials	pMC	Raw ^{14}C age (yr BP)	Calibrated age (yr BP) (1σ)	δ^{13}C (‰)
KIA24386	58	OM	65.58 ± 0.17	3390 ± 20	3186 ± 24	-18.55 ± 0.04
KIA26327	125	OM	46.65 ± 0.20	6125 ± 35	6504 ± 26	-20.02 ± 0.10
KIA24387	155	OM	31.38 ± 0.13	9310 ± 30	10054 ± 104	-19.50 ± 0.08
KIA26328	175	OM	21.96 ± 0.12	12180 ± 45	13618 ± 104	-17.71 ± 0.18
KIA24388	205	OM	13.94 ± 0.11	15830 ± 60	18646 ± 54	-21.65 ± 0.15
KIA24389	275	OM	9.81 ± 0.12	$18650 + 100(-90)$	21774 ± 194	-18.02 ± 0.10
KIA26329	355	OM	2.76 ± 0.06	28830 ± 180	32857 ± 207	-19.23 ± 0.17

OM – organic matter; pMC – percent modern.

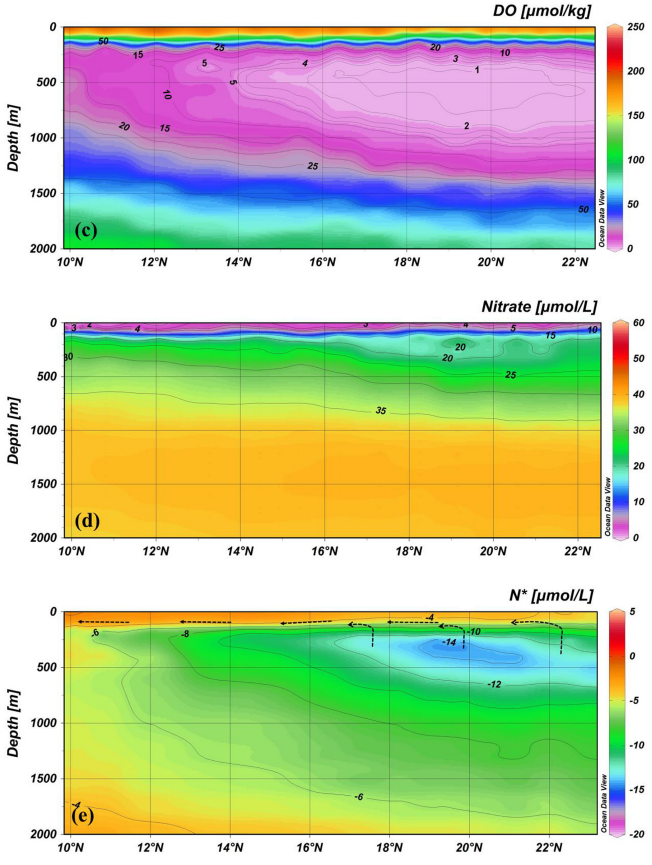

Figure 1. Continued.

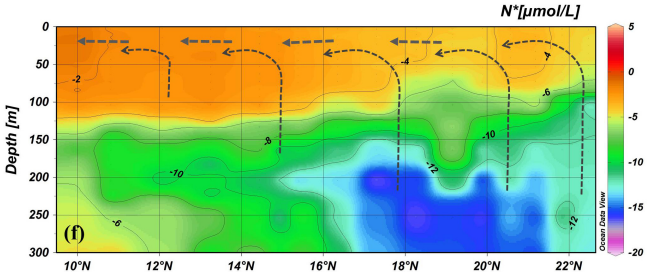

Figure 1. Continued.

precipitationmaximum. In the present day, the SW monsoon is much stronger than its northeastern counterpart.

The spatial distribution of DO at a depth of 150 m for the AS is shown in Fig. 1a (World Ocean Atlas 2009, http://www.nodc.noaa.gov/OC5/WOA09/woa09data.html), which shows a clear southwardly increasing pattern with DO having increased from ~ 5 to $> 100\,\mu\text{mol}\,\text{kg}^{-1}$, and the lowest DO value appears northeast of the northern basin. As denitrification, the dominant nitrate removal process generally occurs in the water column, where DO concentration ranges from 0.7 to $20\,\mu\text{mol}\,\text{kg}^{-1}$ (Paulmier et al., 2009). The intensity of denitrification was reported to descend gradually, corresponding to the DO spatial pattern from the northern to the southern parts of the AS, and did not become obvious at 11 or 12° N (Naqvi et al., 1982). As indicated by the upper 2000 m N–S transect of DO (Fig. 1c), a southwardly decrease in ODZ thickness can be observed and the contour line of $5\,\mu\text{mol}\,\text{kg}^{-1}$ extends to around 13° N. Since the nitrate source is mainly from the bottom of the euphotic zone at around 150 m, we postulate a geographically distinctive sedimentary $\delta^{15}N_{bulk}$ underneath ODZs. Thus, an isopleth of $25\,\mu\text{mol}\,\text{kg}^{-1}$ DO at 150 m is applied as a geographic boundary to separate the northern from the southern part of the AS basin. The interface where DO concentration changed from 20 to $30\,\mu\text{mol}\,\text{kg}^{-1}$ was such a transition zone. On the other hand, the bottom layer of the ODZ moves shallower toward the south, as shown previously by Gouretski and Koltermann (2004). Accordingly, the bottom oxygen content may also be a factor to influence the degree of alteration in sedimentary $\delta^{15}N_{bulk}$.

As mentioned in the introduction, nitrate is removed via denitrification in ODZs resulting in excess P to stimulate N_2 fixation. In Figs. 1d, e and f, we presented the N–S transect of nitrate and N^* (for both the upper 2000 m and 300 m) in January. Even though there is nitrate in the surfacewater

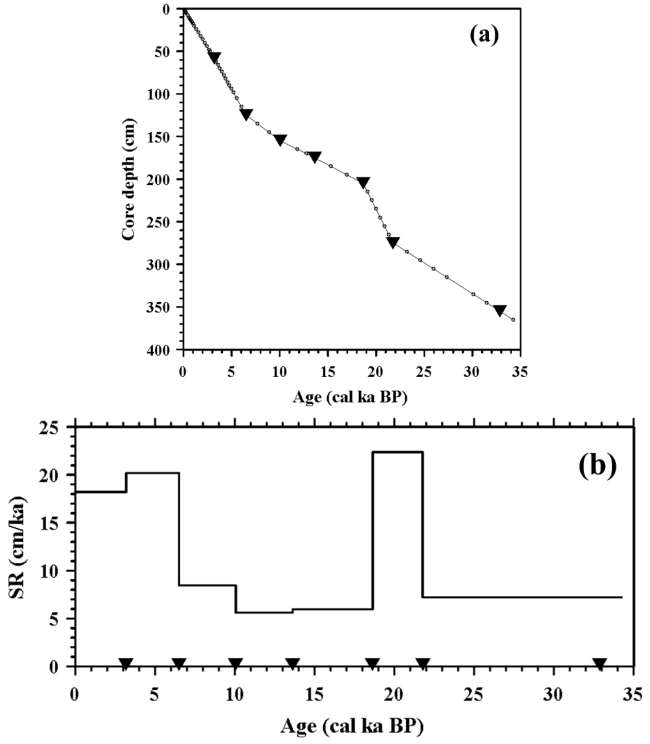

Figure 2. (a) Plot of calendar age against depth; **(b)** Linear sedimentation rate (indicates the ^{14}C age controlling points).

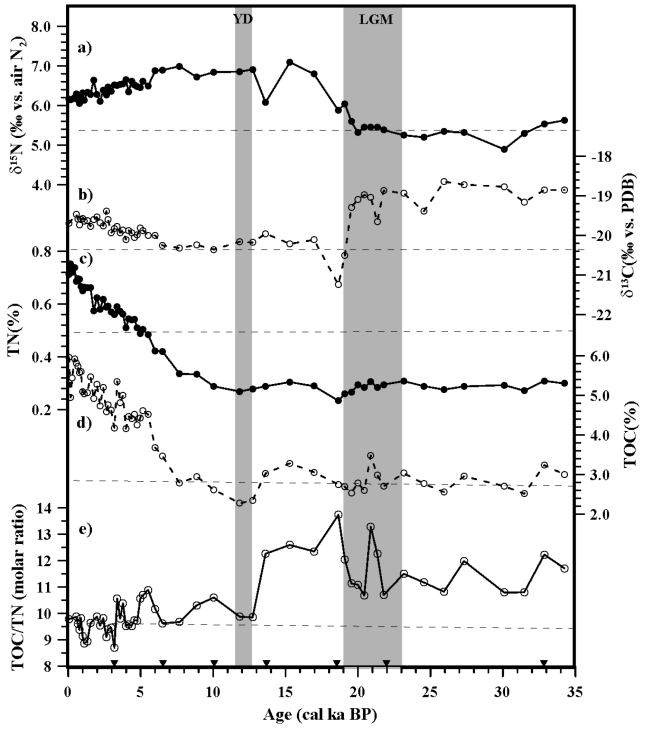

Figure 3. Temporal variations of **(a)** stable isotopic compositions of bulk nitrogen (δ^{15}N); **(b)** stable isotopic compositions of total organic carbon (TOC) (δ^{13}C); **(c)** contents of total nitrogen; **(d)** total organic carbon; **(e)** TOC / TN ratio. Horizontal dashed lines are references for low value periods.

(Fig. 1d), as mentioned earlier, near-surface NO_3^- in the AS is completely utilized in an annual cycle (Altabet, 1988; Thunell et al., 2004). Furthermore, negative N^* (P excess) throughout the water column represents a nitrate deficit, and the lowest N^* value appears at $\sim$ 300 m at 18–20° N, where DO is $< 1\,\mu mol\,kg^{-1}$. Meanwhile, a gradual southwardly increase in N^* can be observed for upper 100 m (Fig. 1f) and the isopleth of N^* of -4 deepens southward with the highest N^* (-2) appearing at $\sim$ 10–12° N. The volume expansion of high N^* water, as well as a simultaneous increase in N^*, strongly indicate an addition of bioavailable nitrogen when surface water is traveling southward.

3 Material and method

A sediment gravity core, SK177/11 (8.2° N and 76.47° E), was collected at water depths of 776 m on the continental slope off the southwest coast of India (Kerala) during the 177th cruise of *ORV SagarKanya* in October 2002. Although the core MD77-191 locates further south in the AS (Bassinot et al., 2012), SK177/11 is, so far, the southernmost core with reference to δ^{15}N record. The 3.65 m long core was subsampled at interval of 2 cm for upper 1 m and of 5 cm for the rest (open circles in Fig. 2a). There is a distinct boundary at $\sim$ 1.7 m, above which the core consists mainly of brownish gray clayey sediments. Neither distinct laminations nor turbidities can be observed by visual contact immediately after collection or at the time during sub-sampling (Pandarinath et al., 2007). All sub-samples were freeze-dried and ground into powder in an agate mortar with pestle. Sand was almost absent (< 1 wt %) throughout the core.

The calendar chronology for core SK177/11 was based on seven accelerator mass spectrometry (AMS) radiocarbon (^{14}C) dates of bulk organic matter (Fig. 2a). Calendar years were calculated using calibration CALIB 6.0 with a reservoir age correction of 402 years (Stuiver et al., 1998; Reimer et al., 2009). Details on the ^{14}C age controlling points were presented in Table 1. Given that the AMS ^{14}C dates of SK177/11 were obtained on total organic carbon (TOC), we may not be able to avoid the mixture of organics of different ages during transport (Mollenhauer et al., 2005) or interference by preaged organics sourced from land (Kao et al., 2008). However, besides the reservoir age correction, due to higher TOC content (range: 2.2–5.5 %) of sediments and their marine-sourced organic carbon, as confirmed by stable C isotope data and C / N ratio, shown in Figs. 3b and e, we are confident that our age model is reliable and less likely affected by age heterogeneity.

Bulk sedimentary nitrogen content and δ^{15}N analyses were carried out using a Carlo-Erba EA 2100 elemental analyzer connected to a Thermo Finnigan Delta V Advantage isotope ratio mass spectrometer (EA-IRMS). Sediments for TOC analyses were acid-treated with 1N HCl for 16 h, and then centrifuged to remove carbonate. The acid-treated sediments were further dried at 60 °C for TOC content and δ^{13}C. The nitrogen isotopic compositions of acidified samples were obtained at the same time for comparison. Carbon and nitrogen isotopic data were presented by standard δ notation with respect to PDB (Pee Dee Belemnite) carbon and atmospheric nitrogen. USGS 40, which has certified δ^{13}C of -26.24 and δ^{15}N of -4.52 ‰ and acetanilide (Merck) with δ^{13}C of -29.76 and δ^{15}N of -1.52 ‰ were used as working standards. The reproducibility of carbon and nitrogen isotopic measurements is better than 0.15 ‰ . The precision of nitrogen and carbon content measurements were better than 0.02 and 0.05 %, respectively. Meanwhile, the acidified and non-acidified samples exhibited identical patterns in δ^{15}N (not shown) with mean deviation of 0.3 ‰.

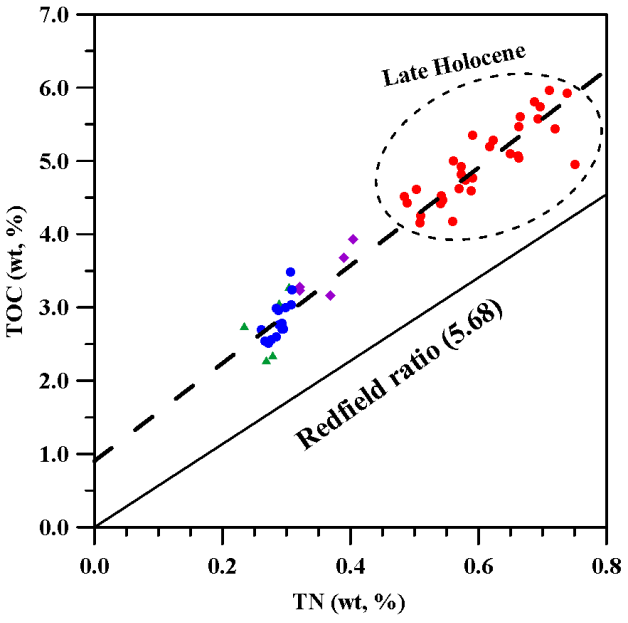

Figure 4. Scatter plot of the total organic carbon content against total nitrogen. Redfield field ratio of 5.68 is shown in line. Bold dashed line stands for regression. Red, purple, green and blue dots represent the late Holocene, early Holocene, deglacial and glacial periods, respectively.

4 Results

4.1 Sedimentation rate

The age–depth curve was shown in Fig. 2a, in which age dates were evenly distributed throughout the core, although not at a high resolution. In Mollenhauer et al. (2005), the largest age offset between total organic carbon and co-occurring foraminifera is $\sim$3000 years and mostly $<$2000 years. Meanwhile, the offset remains more or less constant throughout past 20 ka, regardless of the deglacial transition. The youngest date in our core is 3180 cal ka BP at 58 cm. We may expect younger age on the surface. Thus, if our TOC samples contain any pre-aged organics, as indicated by Mollenhauer et al. (2005), the offset should not be too large to alter our interpretation for the comparison between glacial and Holocene periods. The linear sedimentation rates derived from seven date intervals range from 6 to 20 cm ka^{-1} (Fig. 2b), with relatively constant value ($\sim$6 cm ka^{-1}) prior to Holocene, except for the excursion around the last glacial maximum. The linear sedimentation rates started to increase since Holocene and reached 18–20 cm ka^{-1} when the sea level reached modern-day level.

4.2 Nitrogen and carbon contents and their isotopes

Values of $\delta^{15}N_{bulk}$ ranged from 4.7 to 7.1 ‰ with significantly lower values during the glacial period (Fig. 3a). The δ^{15}N values increased rapidly since $\sim$19 ka BP, with a peak at $\sim$15 ka BP, and then started to decrease gradually toward the modern day, except for the low δ^{15}N excursion at $\sim$14 ka BP. Figure 3b shows that values of $\delta^{13}C_{TOC}$ (-21.5 to -18.5 ‰) were consistent with the δ^{13}C of typical marine organic matter end member (-22 to -18 ‰; Meyers, 1997). An abrupt decrease in δ^{13}C was observed in concert with the dramatic increase in $\delta^{15}N_{bulk}$ at the start of deglaciation.

Bulk nitrogen content (TN) had a range of 0.23–0.75 % (Fig. 3c), and the TOC content ranged from 2.2 to 5.5 % (Fig. 3d). Both TN and TOC showed similar trends over the last 35 ka BP with relatively constant values prior to Holocene and an afterward elevation until the modern day. The upward increasing TOC and TN patterns since Holocene were consistent with the increasing pattern of the sedimentation rate, suggesting a higher organic burial flux induced by enhanced productivity, which had been reported elsewhere in the AS (Altabet et al., 2002).

As for the TOC / TN ratio, higher values appeared during the deglacial transition and the glacial period (Fig. 3e). The highest value coincides with the $\delta^{13}C_{TOC}$ drop, implying that there is still some influence from terrestrial organics. However, terrestrial organics contain less nitrogen (C / N of 20; Meyers, 1997), thus the δ^{15}N did not drop correspondingly. In the first meter (since $\sim$5 ka), the downward decreasing pattern of TOC and TN can also be attributed to syn-sedimentary degradation; if so, a downward increasing in TOC / TN should be evident. However, TOC / TN values varied in a narrow range not revealing a significant increasing trend. Nevertheless, δ^{15}N and δ^{13}C did not show concomitant variations with C / N in the first meter or throughout the core. The influence from both organic degradation and changes in terrestrial organic input on isotopic signals is thus limited.

Figure 4 shows the scatter plot of TOC against TN. The slope of the linear regression line for TOC against TN ($TOC = (6.67 \pm 0.22) \times TN + (0.99 \pm 0.11)$, $R^2 = 0.94$, $n = 57$, $p < 0.0001$) is 6.67, again indicating that organic matter is mainly marine-sourced. Although this slope is slightly higher than the Redfield ratio of 5.68 (wt / wt), it is lower than that observed on the East China Sea shelf (7.46; Kao et al., 2003). Meanwhile, the intercept of TN is negative when TOC downs to zero, implying that inorganic nitrogen can be ignored in our core. Obviously, if we force the regression through the origin point, TOC / TN values for samples during the Holocene will have the lower ratios reflecting even less contribution from terrestrial organics.

5 Discussion

5.1 Downward transfer and transformation of N isotopic signal

As mentioned, the signal of sedimentary $\delta^{15}N$ may be altered under different burial conditions. Altabet and Francois (1994) reported little diagenetic alteration of the near-surface $\delta^{15}N$ in the equatorial Pacific, while there was an apparent +5 ‰ enrichment relative to sinking particles in the Southern Ocean, south of the polar front. In the Sargasso Sea, sedimentary $\delta^{15}N$ also enriched by 3–6 ‰ relative to sinking particles (Altabet et al., 2002; Gruber and Galloway, 2008). The degree of alteration was attributed to particle sinking rate and organic matter (OM) preservation (Altabet, 1988). Gaye-Haake et al. (2005) also suggested that low sedimentation rates benefit organic matter decomposition, resulting in a positive shift in bulk sedimentary $\delta^{15}N$ comparing to sinking particles in the South China Sea. Finally, Robinson et al. (2012) concluded that oxygen exposure time at the seafloor is the dominant factor controlling the extent of N isotopic alteration. Thus, it is necessary to follow the track of $\delta^{15}N$ signal to clarify the occurrence of deviation during transfer.

The reported depth profiles of $\delta^{15}N_{NO_3}$ in the AS were shown in Fig. 5, in which $\delta^{15}N_{NO_3}$ values of water depth deeper than 1200 m range narrowly around 6–7 ‰, which is slightly higher than the global average of the deep oceans ((4.8 ± 0.2) ‰ for > 2500 m, Sigman et al., 2000; (5.7 ± 0.7) ‰ for > 1500 m, Liu and Kaplan, 1989). Below the euphotic layer, $\delta^{15}N_{NO_3}$ increases, rapidly peaking at around 200–400 m. The preferential removal of $^{14}NO_3$ by water column denitrification accounts for these subsurface $\delta^{15}N_{NO_3}$ highs (Brandes et al., 1998; Altabet et al., 1999; Naqvi et al., 2006). The subsurface $\delta^{15}N_{NO_3}$ maximum ranges from 10 to 18 ‰ for different stations, implying a great spatial heterogeneity in water columns denitrification intensity. It is worth mentioning that higher values, in general, appear in the northeastern AS (15 ~ 18 ‰) (Fig. 5), highlighting that the focal area of water column denitrification is prone to the northeastern Arabian Sea (Naqvi et al., 1994; Pichevin et al., 2007), also revealed by the DO spatial distribution (Fig. 1a). Contrary to higher denitrification in the northeastern AS, the export production is always higher in the northwestern AS throughout a year (Rixen et al., 1996). Such decoupling between productivity and denitrification was attributed to the oxygen supply by intermediate water exchange besides primary productivity oxygen demand (Pichevin et al., 2007). Note that the $\delta^{15}N_{NO_3}$ values at a water depth of 100–150 m, which correspond to the bottom depth of the euphotic zone (Olson et al., 1993), from different stations fall within a narrow range of 7–9 ‰ despite wide denitrification intensity underneath. The rapid addition of new nitrogen, as mentioned earlier, might account for the relatively uniform $\delta^{15}N_{NO_3}$ at the bottom of the euphotic layer. Unfortunately, there are no $\delta^{15}N_{NO_3}$ profiles or sediment trap data from the southern basin for comparison.

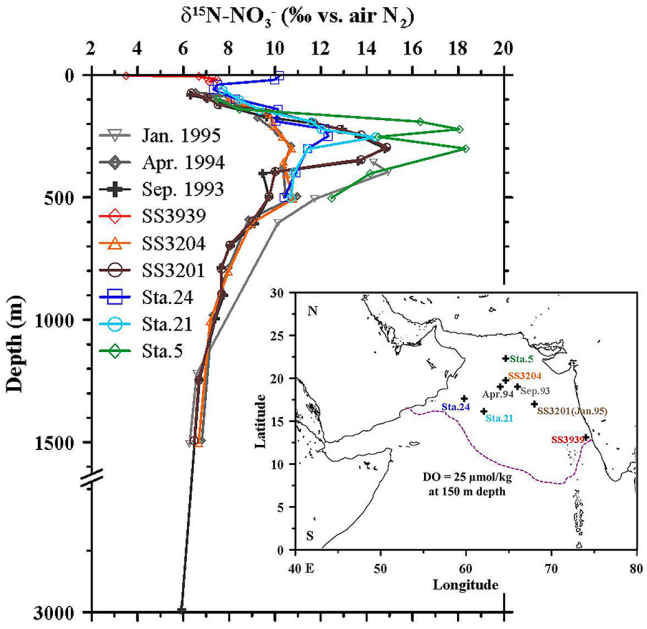

Figure 5. Depth profiles of nitrogen isotope of nitrate ($\delta^{15}N_{NO_3}$) in water columns; data not marked are all from August; the location of Station January 1995 overlaps with Station SS3201 (data digitized from Brandes et al., 1998; Altabet et al., 1999; Naqvi et al., 2006).

Interestingly, reported $\delta^{15}N$ of sinking particles ($\delta^{15}N_{SP}$) collected by five sedimentation traps deployed from 500 m throughout a depth of 3200 m ranged narrowly from 5.1 to 8.5 ‰ (Fig. 6), which is slightly lower but overlaps largely with $\delta^{15}N_{NO_3}$ values at 100–150 m. Such similarity in $\delta^{15}N_{NO_3}$ at 100–150 m and sinking particles strongly indicated that (1) the NO_3^- source for sinking particles was coming from a depth of around 100-150 m, instead of the ODZs (200-400 m) where the maximum $\delta^{15}N_{NO_3}$ value occurred (Schäfer and Ittekkot, 1993; Altabet et al., 1999), and (2) little alteration had occurred in $\delta^{15}N_{SP}$ during sinking in the

water column, as indicated by Altabet (2006). Only these five trap stations with nitrogen isotope information were available in the AS (Gaye-Haaake et al., 2005). The trap locations were in the same area but not as far south compared to the $\delta^{15}N_{NO_3}$ stations (insert map in Fig. 6). The slightly lower $\delta^{15}N$ in sinking particles is attributable to their geographic locations (see below), since incomplete relative utilization of surface nitrate has been documented to have a very limited imprint on the $\delta^{15}N$ signal in the AS (e.g., Schäfer and Ittekkot, 1993).

The uniformly low values of $\delta^{15}N_{NO_3}$ at the bottom of the euphotic zone should be a consequence resulting from various processes in the euphotic zone, such as remineralization, nitrification and N_2 fixation. Nevertheless, the distribution pattern of N^* (Figs. 1e and f) illustrates that there must be an addition of $^{14}NO_3$ into the system to cancel out the isotopic enrichment caused by denitrification. Note that the positive offset in $\delta^{15}N_{NO_3}$ ($\Delta\delta^{15}N_{NO_3}$, 6∼ 12 ‰) in ODZs caused by various degrees of denitrification was narrowed down significantly, while nitrate was transported upward. This implies that a certain degree of addition processes, most likely the N_2 fixation, varied in concert with the intensity of denitrification underneath. Since the upwelling zones distribute at the very north and the west of the AS and the upwelled water travels southward (or outward) on the surface, as shown in Fig. 1e, it is reasonable to see the phenomenon of denitrification-induced N_2 fixation to compensate the nitrogen deficiency. Consistent to this notion, Deutsch et al. (2007) discovered the spatial coupling between denitrification in eastern tropical Pacific (upstream) and N_2 fixation in western equatorial Pacific (downstream). Such a horizontal nitrogen addition process can also be seen clearly in our background information of N^* (Fig. 1f). In fact, fixed N had been proved to account for a significant part of surface nitrate in the modern-day AS, where denitrification is exceptionally intense (Brandes et al., 1998; Capone et al., 1998; Parab et al., 2012).

Compared with reported $\delta^{15}N$ of surface sediments retrieved from trap locations, a significant positive shift in $\delta^{15}N$ can be seen at the seafloor (Fig. 6). Such a positive deviation can be seen elsewhere in previous reports (Altabet, 1988; Brummer et al., 2002; Kienast et al., 2005) due to prolonged oxygen exposure after deposition (Robinsson et al., 2012) associated with sedimentation rate (Pichevin et al., 2007). Although Cowie et al. (2009) found an ambiguous relation between contents of sedimentary organic carbon and oxygen in deep water, they also noticed the appearance of maximum organic carbon contents at the lower boundary of ODZs, where oxygen content was relatively higher. Accordingly, they believed that other factors controlling the preservation of organic carbon existed, such as the chemical characteristics of organic matter, the interaction between organic matters and minerals, the enrichment and activity of benthic organism or the physical factor, including the screening and water dynamic effect.

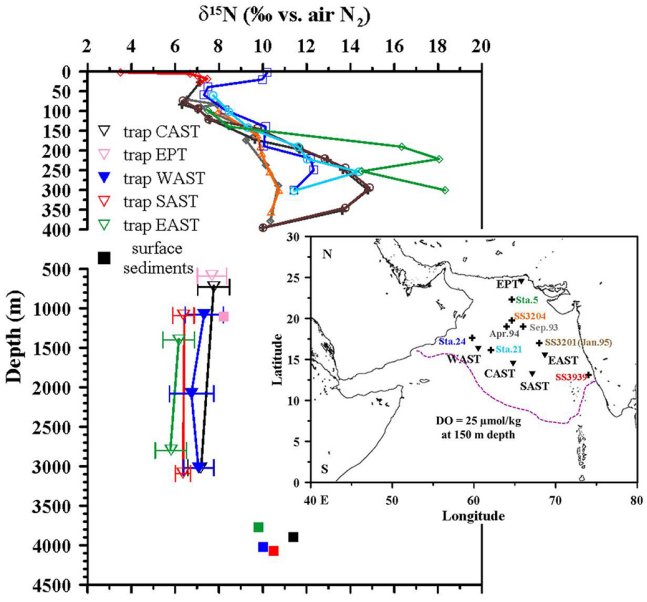

Figure 6. Vertical profiles for nitrogen isotope of nitrate (crosses in inserted map), sinking particles (inverse triangles in map) and trap-corresponding surface sediments. Data for sediment traps and surface sediments are from Gaye-Haake et al. (2005). Depth profile of $\delta^{15}N_{NO_3}$ follows that in Fig. 5.

5.2 Geographically distinctive bottom-depth effects in the modern day

As classified by oxygen content of 25 µmol kg^{-1} at 150 m, the documented surface sedimentary $\delta^{15}N_{bulk}$ (Gaye-Haake et al., 2005) was separated into northern and southern groups to examine the geographic difference in bottom-depth effect. Both groups exhibit positive linear relationships between $\delta^{15}N_{bulk}$ and bottom depth (deeper than 200 m) (Fig. 7a). The regression equations were shown in Table 2. Interestingly, the regressions generally differ statistically from each other in terms of slope and intercept. The slope represents the degree of positive shift of sedimentary $\delta^{15}N$ due to bottom-depth effect. For the southern AS, the slope is (0.76 ($\pm$0.14) $\times$ 10^{-3} km^{-1}), which is close to the correction factor (0.75 $\times$ 10^{-3} km^{-1}) for the world ocean, proposed by Robinson et al. (2012) and further applied by Galbraith et al. (2012). By contrast, the slope for the northern AS is significantly lower (0.55 ($\pm$0.08) $\times$ 10^{-3} km^{-1}), implying that the depth-associated alteration in the northern AS is smaller. The correction factor for bottom-depth effect was predicted to vary in different regions such as that in the South China Sea (Gaye et al., 2009). Since the magnitude of oxygen exposure is the primary control of depth effect (Gaye-Haake et al., 2005; Mobius et al., 2011; Robinson et al., 2012), we attributed this lower slope in the northern AS to relatively higher sedimentation rates (not shown) and lower

Table 2. Linear equations of bottom-depth effect during different climate stages.

Location	Northern AS	Southern AS
Modern	$\delta^{15}N = 0.55\ (\pm 0.08) \times 10^{-3} \times \text{depth} + 8.1\ (\pm 0.2)$ ($R^2 = 0.40, n = 78, P < 0.0001$)	$\delta^{15}N = 0.76\ (\pm 0.14) \times 10^{-3} \times \text{depth} + 6.0\ (\pm 0.3)$ ($R^2 = 0.66, n = 18, P < 0.0001$)
Holocene	$\delta^{15}N = 0.70\ (\pm 0.20) \times 10^{-3} \times \text{depth} + 6.7\ (\pm 0.3)$ ($R^2 = 0.61, n = 16, P = 0.0067$)	$\delta^{15}N = 0.93\ (\pm 0.06) \times 10^{-3} \times \text{depth} + 5.7\ (\pm 0.1)$ ($R^2 = 1.00, n = 3, P = 0.0152$)
Glacial	$\delta^{15}N = 0.64\ (\pm 0.20) \times 10^{-3} \times \text{depth} + 5.2\ (\pm 0.3)$ ($R^2 = 0.68, n = 16, P = 0.0013$)	$\delta^{15}N = 1.01\ (\pm 0.31) \times 10^{-3} \times \text{depth} + 4.3\ (\pm 0.7)$ ($R^2 = 0.91, n = 3, P = 0.1899$*)

* Insignificant by P value.

oxygen contents, as indicated by previous research (Olson et al., 1993; Morrison et al., 1999; Brummer et al., 2002).

On the other hand, the intercept for the northern AS regression (8.1 ± 0.2) is significantly higher than that for the southern AS (6.0 ± 0.3). As mentioned above, $\delta^{15}N$ values of sinking particle resembled the $\delta^{15}N$ of nitrate sourced from a depth of 100–150 m. According to the depth-dependent correction factor, we may convert sedimentary $\delta^{15}N_{bulk}$ values at various water depths into their initial condition when the digenetic alteration is minimal to represent the $\delta^{15}N$ of source nitrate. Higher intercept suggests that a stronger denitrification had occurred in northern AS surface sediments. The 2.1 ‰ lower intercept in the southern AS likely reflects the addition of N_2 fixation in the upper water column while it travels southward. The progressive increase of N^* toward the southern AS supports our speculation, although no $\delta^{15}N_{NO_3}$ profiles had been published in the southern basin. Future works about $\delta^{15}N_{NO_3}$ and $\delta^{15}N_{SP}$ in the southern AS are needed.

In Fig. 7b, we presented corrected $\delta^{15}N_{bulk}$ values along with bottom depth for the northern and southern AS surface sediments for comparison. After removing site-specific bias caused by bottom-depth effect, the values and distribution ranges of $\delta^{15}N_{bulk}$ for both the northern and southern AS became smaller and narrower. For the northern AS, the distribution pattern skewed negatively, giving a standard deviation of 0.88 ‰, falling exactly in the range of 7–9 ‰ for $\delta^{15}N_{NO_3}$ (7–9 ‰) at the bottom of the euphotic zone. As a result, the corrected nitrogen isotopic signals in sediments more truthfully represent the $\delta^{15}N_{NO_3}$ value at the bottom depth of the euphotic zone. Meanwhile, the statistically significant difference in $\delta^{15}N_{bulk}$ distribution between the northern and southern AS further confirms the feasibility of our classification by using DO isopleth of 25 µmol kg^{-1} at 150 m.

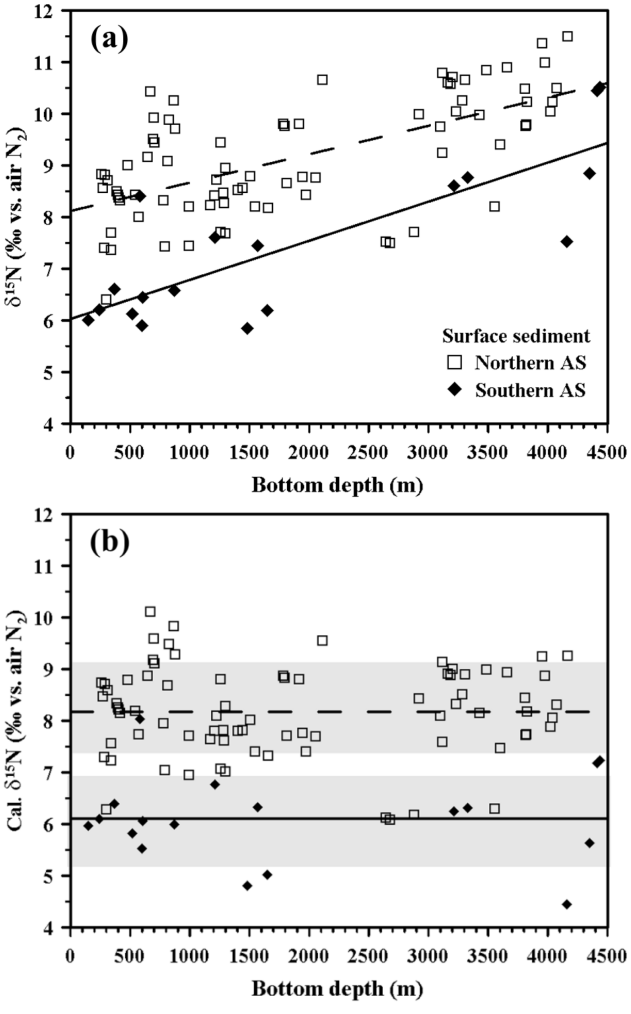

Figure 7. (a) Non-corrected $\delta^{15}N$ values of modern surface sediments against corresponding bottom depth in the northern and southern Arabian Sea (see text for N–S boundary). Regression lines were shown in dashed and solid lines, respectively, for the northern and southern AS. **(b)** Corrected surface sedimentary $\delta^{15}N$ values against water depth.

5.3 Bottom-depth effect during different climate stages

In order to better decipher the history of $\delta^{15}N_{NO_3}$ in the bottom the euphotic zone of the water column, we synthesized almost all available $\delta^{15}N_{bulk}$ of sediment cores reported for the AS (see Figs. 1a and 1b for locations). Similar to modern surface sediments, northern and southern groups were defined by the contour line of 25 µmol kg^{-1} DO. To keep data consistency in the temporal scale, we focused on the last

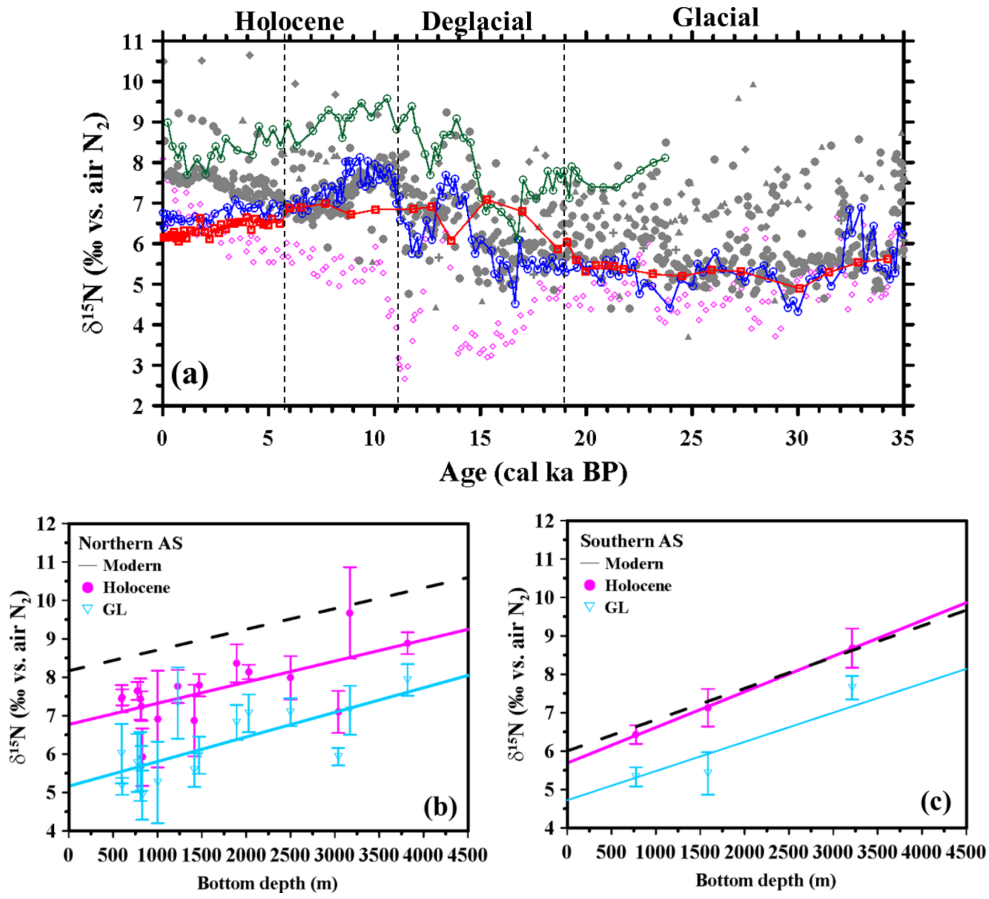

Figure 8. (a) Temporal variations of non-corrected $\delta^{15}N_{bulk}$ values of all reported cores in the AS. Data shown in curves are for cores in the southern Arabian Sea (red for SK177/11, blue for NIOP 905 and green for SO42-74KL), dots in gray are for the northern part and pink dots are for core MD-04-2876. Mean values of $\delta^{15}N$ for fixed periods against corresponding water depths for cores in the **(b)** northern and **(c)** southern Arabian Sea. Pink and indigo blue are for the Holocene and glacial periods, respectively. Error bars represent the standard deviation for mean $\delta^{15}N_{bulk}$.The dashed regression lines for modern surface sediments are shown for reference.

35 ka (Fig. 8a). Unfortunately, data points were less in 0–6 ka and there were only three sediment cores in the southern AS: SK177/11 in this study, and NIOP 905 and SO42-74KL in previous studies.

As shown in Fig. 8a, the original $\delta^{15}N_{bulk}$ from the northern (gray dots) and southern AS (green, blue and red curves) scatter in a wide range from 4.5 to 10.5 ‰ over the entire 35 ka. The pink dots are for the data from core MD-04-2876, which is peculiar since the relatively low $\delta^{15}N_{bulk}$ values deviated from all other reports in the northern AS. Pichevin et al. (2007) excluded the influences from incomplete nitrate utilization and terrestrial input, thus we still include this core in our statistical analyses. As for the southern cores, the temporal variations of $\delta^{15}N_{bulk}$ in core SK177/11 and NIOP 905 (red and blue) had a very similar trend distributing at the lower bound of the whole data set. The mean $\delta^{15}N_{bulk}$ values for SK177/11 and NIOP 905 during the glacial period were almost identical, and the deviation in the Holocene was as small as 0.7 ‰. By contrast, the temporal pattern for $\delta^{15}N_{bulk}$ of core SO42-74KL (green) resembles that of NIOP 905, yet with an enrichment in ^{15}N by $\sim$ 2 ‰ for the entire period. The core SO42-74KL is retrieved from a depth of 3212 m, which is the deepest of the three cores in the southern AS; the positive offset is apparently caused by the bottom-depth effect. Thus, inference should be made with caution when compare sediment cores from different depths.

Below we consider two time spans – 0 $\sim$ 11 ka (Holocene) and 19$\sim$ 35 ka (glacial) – to examine the bottom-depth effect at different climate stages. We ignore the transgression period, which is shorter with more variable in $\delta^{15}N_{bulk}$, to avoid bias caused by dating uncertainties in different studies. Also, we will discuss the peculiar patters for 0–6 ka later. The mean and standard deviation of reported $\delta^{15}N_{bulk}$ values for the specific time span were plotted against the corresponding depth of the core. Accordingly, we obtained the correction factors for glacial and early Holocene, respectively, for the northern and southern AS (Fig. 8b and c). Since only 35 ka was applied in this practice, the long-term alteration (Re-

ichart et al., 1998; Altabet et al., 1999) is ignored. The regression curves for the modern day (dashed lines) were plotted for comparison.

The difference among regressions of three climate stages in the northern AS (Table 2) is not significant (0.55×10^{-3} km^{-1} to 0.70×10^{-3} km^{-1}). However, the regression slopes for the northern AS are significantly lower compared with those obtained from the southern AS for all climate states. This might indicate that the oxygen content in the northern AS is always lower, resulting in a lower degree of alteration of $\delta^{15}N_{bulk}$. On the other hand, we may not exclude the effect by sedimentation rate changes over these two stages, which also affect the oxygen exposure time; unfortunately, insufficient sedimentation rate data in the northern AS in previous reports prevent us from implementing further analysis.

As for the southern AS, correction factors are always higher than those in the northern AS. The overall spatial–temporal patterns are consistent with the oxygen distribution in the Arabian Sea (Olson et al., 1993; Morrison et al., 1999; Pichevin et al., 2007) and agree with the view that DO concentration was the dominant factor for organic matter preservation (Aller, 2001; Zonneveld et al., 2010). Meanwhile, the regression slopes remained high from 0.76×10^{-3} to 1.01×10^{-3} km^{-1} over different climate stages in the southern AS, suggesting that environmental situations, and thus those correction factor, change less relatively to that in the northern AS. For SK177/11, the sedimentation rate in Holocene is two-fold higher compared to that in the glacial period. However, the influence caused by the sedimentation rate changes is likely not significant enough to alter the regression slopes for the southern AS, based on the small changes in the slope (0.93×10^{-3} and 1.01×10^{-3} km^{-1}).

5.4 Insights from temporal changes in geographic $\delta^{15}N_{bulk}$ distribution

Based on the earlier comparison among $\delta^{15}N_{NO_3}$, sinking particles and surface sediments, we recognized that the regression intercept is representative of the nitrogen isotope of nitrate source at a depth of 100 m. Therefore, the regression-derived intercepts given in Table 2 can be used to infer the $\delta^{15}N_{NO_3}$ source at different climate stages, while the slopes can be used as correction factors to eliminate the positive shift in $\delta^{15}N_{bulk}$ caused by bottom depth; by doing this, we can get the original signal of $\delta^{15}N_{bulk}$ prior to alteration. We applied the correction factor to be equal to (bottom depth -100 m) $\times$ slope, ignoring the sea level changes during the different climate stages.

Noticeably, the regression intercepts for both the northern and southern AS are higher in the Holocene compared to those in the glacial period, indicating the intensified isotopic enrichment in $\delta^{15}N_{NO_3}$ in the entire AS in Holocene. Such increment is almost the same to be ~ 1.5 ‰, which is similar to the increase in the eastern tropical North Pacific, but slightly smaller than that in the eastern tropical South Pacific (Galbraith et al., 2012). The 120 m sea level increase, which may induce only a 0.1 ‰ offset, cannot be the reason for such a significant increase of average $\delta^{15}N_{bulk}$ during the Holocene. Moreover, deviations between the northern and southern AS at the respective climate stage are almost identical (1.0 ‰ for Holocene and 0.9 ‰ for glacial), indicating a synchronous shift in the relative intensity of denitrification and N_2 fixation over the basin to keep such a constant latitudinal gradient of subsurface $\delta^{15}N_{NO_3}$.

The intermediate water formation near the polar region controls the oxygen supply to the intermediate water and thus the extent of denitrification on global scale and the stoichiometry of nutrient source to the euphotic zone (Galbraith et al., 2004). Lower glacial-stage sea surface temperature may increase oxygen solubility, while stronger winds in high-latitude regions enhance the rate of thermocline ventilation. The resultant colder and rapidly flushed thermocline thus lessened the spatial extent of denitrification and, consequently, N fixation (Galbraith et al., 2004). Therefore, such a basin of wide synchronous increase in $\delta^{15}N_{bulk}$ is likely a global control. The lower intercepts in glacial time (4.3 ‰ for the south and 5.3 ‰ for the north), which are similar to the global mean $\delta^{15}N_{NO_3}$ (4.5–5 ‰, Sigman et al., 1997), illustrate a better ventilation of intermediate water during glacial time in the Arabian Sea (Pichevin et al., 2007). In fact, the AAIWs penetrate further northward over 5° N in the present day and even during the late Holocene (You, 1998; Pichevin et al., 2007). Since the $\delta^{13}C$ of autochthonous particulate organic carbon is negatively correlated to [CO_2 (aq)] in the euphotic zone (Rau et al., 1991), the sharp decrease of $\delta^{13}C_{TOC}$ in SK177/11 at the start of deglaciation (Fig. 3b) may infer the timing of a rapid accumulation of dissolved inorganic carbon driven by the shrinking of oxygenated intermediate water (Pichevin et al., 2007) or enhanced monsoon-driven upwelling (Ganeshram et al., 2000); both facilitate the promotion of denitrification. Nevertheless, the mirror image between $\delta^{15}N$ and $\delta^{13}C_{TOC}$ pro?les revealed their intimate relation, of which the variability was attributable to the change of physical processes.

The intercepts of the northern AS increase continuously from 5.2 to 8.1 from glacial through to modern day, indicating the strengthened intensity of denitrification relative to nitrogen fixation in the northern AS (Altabet, 2007). When we take a close look at the temporal pattern of corrected $\delta^{15}N_{bulk}$ for long cores (Fig. 9), we can see an amplified deviation since 6 ka, during which $\delta^{15}N_{bulk}$ increases continuously in the northern AS, whereas it decreases in the southern AS. Note that the northern most core, MD-04-2876, also followed the increasing trend in recent 6 ka even though its $\delta^{15}N_{bulk}$ values deviated from all other cores. Such opposite trends indicate that the controlling factors on the nitrogen cycle in the northern AS were different from that in the southern AS, which means that localized enhancement in specific process had occurred.

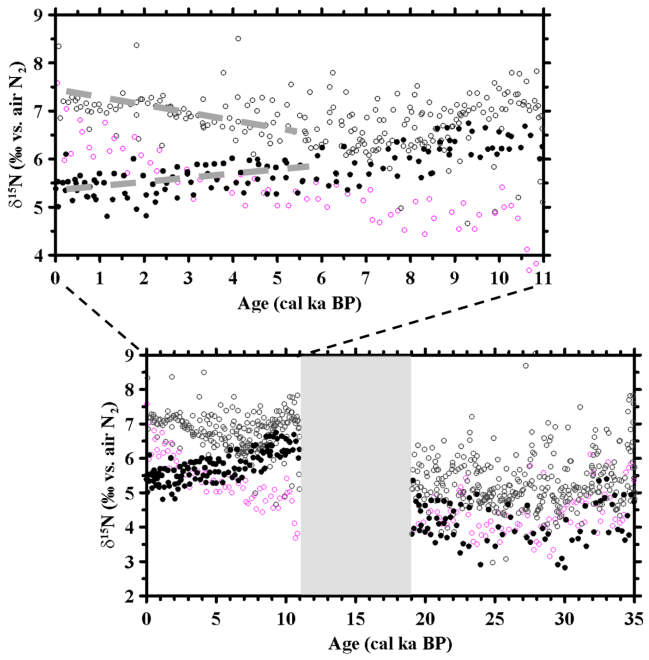

Figure 9. Temporal variations of corrected $\delta^{15}N_{bulk}$ values of all reported cores in the AS. Gray and black dots are for the northern and southern AS, respectively. Pink dots are specifically for core MD-04-2876. The deglacial period is in shadow because non proper equations for bottom-depth effect correction. The upper panel is the blow-up for the Holocene period. The intensified deviation trends since 6 ka were marked by bold dashed lines.

Besides the oxygen supply to the intermediate water, the intensity of water column denitrification varies with primary productivity (Altabet, 2006; Naqvi et al., 2006). Strong summer monsoon and winter monsoon drive upwelling or convective mixing enhances primary productivity, which, in turn, intensifies denitrification (Altabet et al., 2002; Ganeshram et al., 2002). However, it was also reported that primary productivity did not correlate well with water column denitrification underneath during the Holocene in some parts of the northern AS (Banakar et al., 2005, and references therein). Regardless of the declining summer monsoon strength since 5500 ka (Hong et al., 2003), primary productivity in the northern AS seemed to have increased. Similar to the patterns observed for TOC and TN in this study, productivity indicators (TOC and Ba / Al ratios), reported by Rao et al. (2010) in the core SK148/4 located near our SK177/11, also increased gradually since the Holocene. Incomplete nitrate consumption can hardly explain the decreasing pattern for all three cores in the southern AS, where upwelling intensity is much less relative to that in the north. Moreover, lower TOC / TN ratios observed in Holocene in SK177/11, as mentioned earlier, rule out the influence of terrestrial organic input. Therefore, a spatial coupling of denitrification-dependent N_2 fixation is the more plausible cause of the decreasing $\delta^{15}N_{bulk}$ pattern (Deutsch et al., 2007).

We suggested that the intensified supply of excess phosphorous (phosphorus in stoichiometric excess of fixed nitrogen) toward the southern AS to stimulate N_2 fixation, subsequently responsible for the decreasing $\delta^{15}N_{bulk}$ pattern in the southern basin. The intensification in excess phosphorous supply can be driven by enhanced upwelling or intensified subsurface water column denitrification or both. According to the increasing pattern in $\delta^{15}N_{bulk}$ and primary productivity in the northern AS, synergetic processes are suggested. The upwelled water in the northern AS basin brings up low N / P water to the surface for non-diazotrophs to uptake. If we assume complete consumption, the remaining excess phosphorous after complete consumption will be transported toward the south by clockwise surface circulation and advection. Therefore, N_2 fixation in the southern AS acts as feedback to balance denitrification changes in the northern AS. This phenomenon is similar to the illustration for the spatial coupling of nitrogen inputs and losses in the Pacific Ocean, proposed by Deutsch et al. (2007). The question as to why such forcing to expand the N–S deviation had not occurred before 6 ka warrants more studies.

6 Conclusions

The available data showed that values of $\delta^{15}N_{NO_3}$ at the bottom of the euphotic zone ($\sim$ 150 m) were similar to $\delta^{15}N_{SP}$, implying that the source of nutrients for sinking particulate organic matter was largely derived from a depth of around 150 m. Values of sedimentary $\delta^{15}N_{bulk}$ were obviously higher than $\delta^{15}N_{SP}$ in surrounding areas, suggesting that such a shift of sedimentary $\delta^{15}N_{bulk}$ occurred after deposition. It is necessary to remove site-specific bias of $\delta^{15}N_{bulk}$ values caused by bottom depth to retrieve the original signal before alteration. As a result, the corrected nitrogen isotopic signal in sediments could be representative of the value of $\delta^{15}N_{NO_3}$ at the bottom depth of the euphotic zone. The bottom-depth effects in the northern AS vary during different climate stages, but the variation is always lower than such effects in the southern AS in general. The modern surface $\delta^{15}N_{bulk}$ values can be separated statistically into northern and southern AS groups, reflecting a special coupling of denitrification to the north, and N_2 fixation to the south. This phenomenon is supported by the reported modern-day N^* distribution. As for historical records, the offset in $\delta^{15}N_{bulk}$ between the southern and northern AS remained relatively constant (1.0 ‰ for early Holocene and 0.9 ‰ for glacial) prior to 6 ka, indicating a synchronous shift in the relative intensity of denitrification and N_2 fixation over the basin to keep such a constant latitudinal gradient of subsurface $\delta^{15}N_{NO_3}$. However, this offset expanded gradually since 6 ka, likely due to more localized intensifications in denitrification and N_2 fixation had occurred, respectively, in the northern and southern Arabian Seas. The spatial coupling of nitrogen inputs and losses in the Arabian Sea was proposed, yet the

question as to why the driving force did not expand the N–S deviation before 6 ka warrants more studies.

Acknowledgements. This research was supported by the National Natural Science Foundation of China (NSFC 41176059, 91328207, and 41273083) and Shanhai Fund (2013SH012). K. Selvaraj personally thanks the director of the National Center for Antarctic and Ocean Research, Goa and the Secretary, the Department of Ocean Development, New Delhi, for providing the ship time, and also the crew of *ORV Sagar Kanya* for coring operation. K. Selvaraj also thanks V. Yoganandan for onboard help of subsampling, and the coordinator of Ocean Science and Technology Cell of Mangalore University, for their kind encouragement.

Edited by: N. Ohkouchi

References

Agnihotri, R., Altabet, M. A., and Herbert, T.: Influence of marine denitrification on atmospheric N_2O variability during the Holocene, Geophys. Res. Lett., 33, , L13704, doi:10.1029/2006GL025864, 2006.

Aller, R. C.: Transport and reactions in the bioirrigated zone, The benthic boundary layer: Transport processes and biogeochemistry, edited by: B. Boudreau, and Jørgensen, B. B., Oxford University Press, Oxford, UK, 269–301, 2001.

Altabet, M.: Variations in nitrogen isotopic composition between sinking and suspended particles: Implications for nitrogen cycling and particle transformation in the open ocean, Deep-Sea Res. Pt. A, 35, 535–554, 1988.

Altabet, M. and Francois, R.: Sedimentary nitrogen isotopic ratio as a recorder for surface ocean nitrate utilization, Global Biogeochem. Cy., 8, 103–116, 1994.

Altabet, M., Francois, R., Murray, D. W., and Prell, W. L.: Climate-related variations in denitrification in the Arabian Sea from sediment $^{15}N/^{14}N$ ratios, Nature, 373, 506–509, 1995.

Altabet, M., Murray, D. W., and Prell, W. L.: Climatically linked oscillations in Arabian Sea denitrification over the past 1 my: Implications for the marine N cycle, Paleoceanography, 14, 732–743, 1999.

Altabet, M., Higginson, M. J., and Murray, D. W.: The effect of millennial-scale changes in Arabian Sea denitrification on atmospheric CO_2, Nature, 415, 159–162, 2002.

Altabet, M.: Isotopic tracers of the marine nitrogen cycle: Present and past, in: Marine organic matter: biomarkers, isotopes and DNA, edited by: Volkman, J. K., Springer-Verlag Berlin Heidelberg, 251–293, 2006.

Altabet, M.: Constraints on oceanic N balance/imbalance from sedimentary ^{15}N records, Biogeosciences, 4, 75–86, 2007, http://www.biogeosciences.net/4/75/2007/.

Banakar, V., Oba, T., Chodankar, A., Kuramoto, T., Yamamoto, M., and Minagawa, M.: Monsoon related changes in sea surface productivity and water column denitrification in the Eastern Arabian Sea during the last glacial cycle, Mar. Geol., 219, 99–108, 2005.

Bassinot, F. C., Marzin, C., Braconnot, P., Marti, O., Mathien-Blard, E., Lombard, F., and Bopp, L.: Holocene evolution of summer winds and marine productivity in the tropical Indian Ocean in response to insolation forcing: data-model comparison, Clim. Past, 7, 815–829, doi:10.5194/cp-7-815-2011, 2011.

Brandes, J. A., Devol, A. H., Yoshinari, T., Jayakumar, D., and Naqvi, S.: Isotopic composition of nitrate in the central Arabian Sea and eastern tropical North Pacific: A tracer for mixing and nitrogen cycles, Limnol. Oceanogr., 43, 1680–1689, 1998.

Brummer, G., Kloosterhuis, H., and Helder, W.: Monsoon-driven export fluxes and early diagenesis of particulate nitrogen and its $\delta^{15}N$ across the Somalia margin, Geological Society, London, Special Publications, 195, 353–370, 2002.

Capone, D. G., Zehr, J. P., Paerl, H. W., Bergman, B., and Carpenter, E. J.: Trichodesmium, a globally significant marine cyanobacterium, Science, 276, 1221-1229, 1997.

Capone, D. G., Subramaniam, A., Montoya, J. P., Voss, M., Humborg, C., Johansen, A. M., Siefert, R. L., and Carpenter, E. J.: An extensive bloom of the N_2-fixing cyanobacterium Trichodesmium erythraeum in the central Arabian Sea, Mari. Ecol.-Prog. Ser., 172, 281–292, 1998.

Codispoti, L. and Christensen, J.: Nitrification, denitrification and nitrous oxide cycling in the eastern tropical South Pacific Ocean, Mar. Chem., 16, 277–300, 1985.

Cowie, G. L., Mowbray, S., Lewis, M., Matheson, H., and McKenzie, R.: Carbon and nitrogen elemental and stable isotopic compositions of surficial sediments from the Pakistan margin of the Arabian Sea, Deep-Sea Res. Pt. II, 56, 271–282, 2009.

Deutsch, C., Sarmiento, J. L., Sigman, D. M., Gruber, N., and Dunne, J. P.: Spatial coupling of nitrogen inputs and losses in the ocean, Nature, 445, 163–167, 2007.

Falkowski, P. G. and Godfrey, L. V.: Electrons, life and the evolution of Earth's oxygen cycle, Philosoph. Trans. Roy. Soc. B, 363, 2705–2716, 2008.

Galbraith, E. D., Kienast, M., Pedersen, T. F., and Calvert, S. E.: Glacial-interglacial modulation of the marine nitrogen cycle by high-latitude O_2 supply to the global thermocline, Paleoceanography, 19, PA4007, doi:10.1029/2003PA00100, 2004.

Galbraith, E. D., Kienast, M., Albuquerque, A. L., Altabet, M., Batista, F., Bianchi, D., Calvert, S., Quintana, S. C., Crosta, X., Holz, R. D. P., Dubois, N., Etourneau, J., Francois, R., Hsu, T.-C., Ivanochko, T., Jaccard, S., Kao, S.-J., Kiefer, T., Kienast, S., Lehmann, M. F., Martinez, P., McCarthy, M., Meckler, A. N., Mix, A., Möbius, J., Pedersen, T., Pichevin, L., Quan, T. M., Robinson, R. S., Ryabenko, E., Schmittner, A., Schneider, R., Schneider-Mor, A., Shigemitsu, M., Sinclair, D., Somes, C., Studer, A., Tesdal, J. E., Thunell, R., and Yang, J.-Y.: The acceleration of oceanic denitrification during deglacial warming, Nat. Geosci., 5, 151–156, 2012.

Ganeshram, R. S., Pedersen, T. F., Calvert, S. E., and Murray, J. W.: Large changes in oceanic nutrient inventories from glacial to interglacial periods, Nature, 376, 755–758, 1995. Ganeshram, R. S., Pedersen, T. F., Calvert, S. E., McNeill, G. W., and Fontugne, M. R.: Glacial-interglacial variability in denitrification in the world's oceans: Causes and consequences, Paleoceanography, 15, 361–376, 2000.

Ganeshram, R. S., Pedersen, T. F., Calvert, S., and François, R.: Reduced nitrogen fixation in the glacial ocean inferred from changes in marine nitrogen and phosphorus inventories, Nature, 415, 156–159, 2002.

Gaye, B., Wiesner, M., and Lahajnar, N.: Nitrogen sources in the South China Sea, as discerned from stable nitrogen isotopic ra-

tios in rivers, sinking particles, and sediments, Marine Chemistry, 114, 72–85, 2009.

Gaye-Haake, B., Lahajnar, N., Emeis, K. C., Unger, D., Rixen, T., Suthhof, A., Ramaswamy, V., Schulz, H., Paropkari, A., and Guptha, M.: Stable nitrogen isotopic ratios of sinking particles and sediments from the northern Indian Ocean, Mar. Chem., 96, 243–255, 2005.

Gouretski, V. and Koltermann, K. P.: WOCE global hydrographic climatology, Berichte des BSH, 35, 1–52, 2004.

Gruber, N. and Sarmiento, J. L.: Biogeochemical/physical interactions in elemental cycles, in: The sea: Biological-Physical Interactions in the Oceans, edited by: Robinson, A. R., McCarthy, J. J., and Rothschild, B. J., John Wiley and Sons, New York, 337–399, 2002.

Gruber, N.: The dynamics of the marine nitrogen cycle and its influence on atmospheric CO_2 variations, in: The ocean carbon cycle and climate, edited by: Follows, M., and Oguz, T., Springer Netherlands, 97–148, 2004.

Gruber, N. and Galloway, J. N.: An Earth-system perspective of the global nitrogen cycle, Nature, 451, 293–296, 2008.

Haug, G. H., Pedersen, T. F., Sigman, D. M., Calvert, S. E., Nielsen, B., and Peterson, L. C.: Glacial/interglacial variations in production and nitrogen fixation in the Cariaco Basin during the last 580 kyr, Paleoceanography, 13, 427–432, 1998.

Holmes, M. E., Schneider, R. R., Müller, P. J., Segl, M., and Wefer, G.: Reconstruction of past nutrient utilization in the eastern Angola Basin based on sedimentary $^{15}N/^{14}N$ ratios, Paleoceanography, 12, 604–614, 1997.

Hong, Y., Hong, B., Lin, Q., Zhu, Y., Shibata, Y., Hirota, M., Uchida, M., Leng, X., Jiang, H., and Xu, H.: Correlation between Indian Ocean summer monsoon and North Atlantic climate during the Holocene, Earth Planet. Sci. Lett., 211, 371–380, 2003.

Ivanochko, T. S., Ganeshram, R. S., Brummer, G. J. A., Ganssen, G., Jung, S. J. A., Moreton, S. G., and Kroon, D.: Variations in tropical convection as an amplifier of global climate change at the millennial scale, Earth Planet. Sci. Lett., 235, 302–314, 2005.

Kao, S., Lin, F., and Liu, K.: Organic carbon and nitrogen contents and their isotopic compositions in surficial sediments from the East China Sea shelf and the southern Okinawa Trough, Deep-Sea Res. Pt. II, 50, 1203–1217, 2003.

Kao, S., Dai, M., Wei, K., Blair, N., and Lyons, W.: Enhanced supply of fossil organic carbon to the Okinawa Trough since the last deglaciation, Paleoceanography, 23, PA2207, doi:10.1029/2007PA001440, 2008.

Kienast, M., Higginson, M., Mollenhauer, G., Eglinton, T. I., Chen, M. T., and Calvert, S. E.: On the sedimentological origin of down-core variations of bulk sedimentary nitrogen isotope ratios, Paleoceanography, 20, PA2009, doi:10.1029/2004PA0018081, 2005.

Liu, K.-K. and Kaplan, I. R.: The eastern tropical Pacific as a source of ^{15}N-enriched nitrate in seawater off southern Califomia, Limnol. Oceanogr, 34, 820–830, 1989.

Meyers, P. A.: Organic geochemical proxies of paleoceanographic, paleolimnologic, and paleoclimatic processes, Organ. Geochem., 27, 213–250, 1997.

Möbius, J., Gaye, B., Lahajnar, N., Bahlmann, E., and Emeis, K.-C.: Influence of diagenesis on sedimentary $\delta^{15}N$ in the Arabian Sea over the last 130kyr, Mar. Geol., 284, 127–138, 2011.

Mollenhauer, G., Kienast, M., Lamy, F., Meggers, H., Schneider, R. R., Hayes, J. M., and Eglinton, T. I.: An evaluation of ^{14}C age relationships between co-occurring foraminifera, alkenones, and total organic carbon in continental margin sediments, Paleoceanography, 20, PA1016, doi:10.1029/2004PA001103, 2005.

Morrison, J., Codispoti, L., Gaurin, S., Jones, B., Manghnani, V., and Zheng, Z.: Seasonal variation of hydrographic and nutrient fields during the US JGOFS Arabian Sea Process Study, Deep-Sea Res. Pt. II, 45, 2053–2101, 1998.

Morrison, J., Codispoti, L., Smith, S. L., Wishner, K., Flagg, C., Gardner, W. D., Gaurin, S., Naqvi, S., Manghnani, V., and Prosperie, L.: The oxygen minimum zone in the Arabian Sea during 1995, Deep-Sea Res. Pt. II, 46, 1903–1931, 1999.

Nair, R., Ittekkot, V., Manganini, S., Ramaswamy, V., Haake, B., Degens, E., Desai, B. t., and Honjo, S.: Increased particle flux to the deep ocean related to monsoons, Nature, 338, 749–751, 1989.

Naqvi, S., Noronha, R. J., and Reddy, C.: Denitrification in the Arabian Sea, Deep-Sea Res. Pt. A, 29, 459–469, 1982.

Naqvi, S.: Denitrification processes in the Arabian Sea, Proc. Ind. Acad. Sci.-Earth Plane. Sci., 103, 279–300, 1994.

Naqvi, S., Naik, H., Pratihary, A., D'Souza, W., Narvekar, P., Jayakumar, D., Devol, A., Yoshinari, T., and Saino, T.: Coastal versus open-ocean denitrification in the Arabian Sea, Biogeosciences, 3, 621–633, 2006, http://www.biogeosciences.net/3/621/2006/.

Olson, D. B., Hitchcock, G. L., Fine, R. A., and Warren, B. A.: Maintenance of the low-oxygen layer in the central Arabian Sea, Deep-Sea Res. Pt. II, 40, 673–685, 1993.

Pandarinath, K., Subrahmanya, K., Yadava, M., and Verma, S.: Late Quaternary Sedimentation Records on the Continental Slope Off Southwest Coast of India-Implications for Provenance, Depositional and Paleomonsoonal Conditions, J. Geol. Soc. India, 69, 1285–1292, 2007.

Parab, S. G. and Matondkar, S.: Primary productivity and nitrogen fixation by *Trichodesmium* spp. in the Arabian Sea, J. Mar. Syst., 105, 82–95, 2012.

Paulmier, A. and Ruiz-Pino, D.: Oxygen minimum zones (OMZs) in the modern ocean, Prog. Oceanogr., 80, 113–128, 2009.

Pichevin, L., Bard, E., Martinez, P., and Billy, I.: Evidence of ventilation changes in the Arabian Sea during the late Quaternary: Implication for denitrification and nitrous oxide emission, Global Biogeochem. Cy., 21, GB4008, doi:10.1029/2006GB002852, 2007.

Rao, V. P., Kessarkar, P. M., Thamban, M., and Patil, S. K.: Paleoclimatic and diagenetic history of the late quaternary sediments in a core from the Southeastern Arabian Sea: Geochemical and magnetic signals, J. Oceanogr., 66, 133–146, 2010.

Rau, G., Froelich, P. N., Takahashi, T., and Des Marais, D.: Does sedimentary organic $\delta^{13}C$ record variations in Quaternary ocean $[CO_2(aq)]$, Paleoceanography, 6, 335–347, 1991.

Reichart, G.-J., Lourens, L., and Zachariasse, W.: Temporal variability in the northern Arabian Sea Oxygen Minimum Zone (OMZ) during the last 225,000 years, Paleoceanography, 13, 607–621, 1998.

Reimer, P. J., Baillie, M. G., Bard, E., Bayliss, A., Beck, J. W., Blackwell, P. G., Ramsey, C. B., Buck, C. E., Burr, G. S., and Edwards, R. L.: IntCal09 and Marine09 radiocarbon age calibra-

tion curves, 0–50 000 yeats cal BP, Radiocarbon, 51, 1111–1150, 2009.

Rixen, T., Haake, B., Ittekkot, V., Guptha, M., Nair, R., and Schlüssel, P.: Coupling between SW monsoon-related surface and deep ocean processes as discerned from continuous particle flux measurements and correlated satellite data, J. Geophys. Res., 101, 28569–28528, 1996.

Robinson, R. S., Brunelle, B. G., and Sigman, D. M.: Revisiting nutrient utilization in the glacial Antarctic: Evidence from a new method for diatom-bound N isotopic analysis, Paleoceanography, 19, PA3001, doi:10.1029/2003PA000996, 2004.

Robinson, R. S., Kienast, M., Luiza Albuquerque, A., Altabet, M., Contreras, S., De Pol Holz, R., Dubois, N., Francois, R., Galbraith, E., and Hsu, T. C.: A review of nitrogen isotopic alteration in marine sediments, Paleoceanography, 27, PA4203, doi:10.1029/2012PA002321, 2012.

Schäfer, P. and Ittekkot, V.: Seasonal variability of δ^{15}N in settling particles in the Arabian Sea and its palaeogeochemical significance, Naturwissenschaften, 80, 511–513, 1993.

Schmittner, A., Galbraith, E. D., Hostetler, S. W., Pedersen, T. F., and Zhang, R.: Large fluctuations of dissolved oxygen in the India and Pacific oceans during Dansgaard-Oeschger oscillations caused by variations of North Atlantic Deep Water subduction, Paleoceanography, 22, PA3207, doi:10.1029/2006PA001384, 2007.

Schubert, C. J. and Calvert, S. E.: Nitrogen and carbon isotopic composition of marine and terrestrial organic matter in Arctic Ocean sediments: implications for nutrient utilization and organic matter composition, Deep-Sea Res. Pt. I, 48, 789–810, 2001.

Schulte, S., Rostek, F., Bard, E., Rullkötter, J., and Marchal, O.: Variations of oxygen-minimum and primary productivity recorded in sediments of the Arabian Sea, Earth Planet. Sci. Lett., 173, 205–221, 1999.

Sigman, D., Altabet, M., Michener, R., McCorkle, D., Fry, B., and Holmes, R.: Natural abundance-level measurement of the nitrogen isotopic composition of oceanic nitrate: an adaptation of the ammonia diffusion method, Mar. Chem., 57, 227–242, 1997.

Sigman, D., Altabet, M., McCorkle, D., Francois, R., and Fischer, G.: The δ^{15}N of nitrate in the Southern Ocean: nitrogen cycling and circulation in the ocean interior, J. Geophys. Res.-Oceans (1978–2012), 105, 19599–19614, 2000.

Sigman, D. M., Karsh, K. L., and Casciotti, K. L.: Nitrogen Isotopes in the Ocean, in: Encyclopedia of Ocean Sciences, edited by: John, H. S. (Editor-in-Chief), Academic Press, Oxford, 1884–1894, 2001.

Stuiver, M. and Braziunas, T. F.: Anthropogenic and solar components of hemispheric ^{14}C, Geophys. Res. Lett., 25, 329–332, 1998.

Suthhof, A., Ittekkot, V., and Gaye-Haake, B.: Millennial-scale oscillation of denitrification intensity in the Arabian Sea during the late Quaternary and its potential influence on atmospheric N_2O and global climate, Global Biogeochem. Cy., 15, 637–649, 2001.

Thunell, R. C., Sigman, D. M., Muller-Karger, F., Astor, Y., and Varela, R.: Nitrogen isotope dynamics of the Cariaco Basin, Venezuela, Global Biogeochem. Cy., 18, GB3001, doi:10.1029/2003GB002185, 2004.

You, Y.: Intermediate water circulation and ventilation of the Indian Ocean derived from water-mass contributions, J. Mar.Res., 56, 1029–1067, 1998.

Zonneveld, K. A. F., Versteegh, G. J. M., Kasten, S., Eglinton, T. I., Emeis, K.-C., Huguet, C., Koch, B. P., de Lange, G. J., de Leeuw, J. W., Middelburg, J. J., Mollenhauer, G., Prahl, F. G., Rethemeyer, J., and Wakeham, S. G.: Selective preservation of organic matter in marine environments; processes and impact on the sedimentary record, Biogeosciences, 7, 483–511, doi:10.5194/bg-7-483-2010, 2010.